

Mapping Dirac quasiparticles near a single Coulomb impurity on graphene

Yang Wang^{1,2†}, Victor W. Brar^{1,2†}, Andrey V. Shytov³, Qiong Wu^{1,2}, William Regan^{1,2}, Hsin-Zon Tsai¹, Alex Zettl^{1,2}, Leonid S. Levitov⁴ and Michael F. Crommie^{1,2*}

The response of Dirac fermions to a Coulomb potential is predicted to differ significantly from how non-relativistic electrons behave in traditional atomic and impurity systems 1-3. Surprisingly, many key theoretical predictions for this ultrarelativistic regime have not been tested⁴⁻¹². Graphene, a twodimensional material in which electrons behave like massless Dirac fermions 13,14, provides a unique opportunity to test such predictions. Graphene's response to a Coulomb potential also offers insight into important material characteristics, including graphene's intrinsic dielectric constant^{6,8}, which is the primary factor determining the strength of electron-electron interactions in graphene¹⁵. Here we present a direct measurement of the nanoscale response of Dirac fermions to a single Coulomb potential placed on a gated graphene device. Scanning tunnelling microscopy was used to fabricate tunable charge impurities on graphene, and to image electronic screening around them for a Q = +1|e| charge state. Electron-like and hole-like Dirac fermions were observed to respond differently to a Coulomb potential. Comparing the observed electron-hole asymmetry to theoretical simulations has allowed us to test predictions for how Dirac fermions behave near a Coulomb potential, as well as extract graphene's intrinsic dielectric constant: $\varepsilon_g = 3.0 \pm 1.0$. This small value of ε_g indicates that electron-electron interactions can contribute significantly to graphene properties.

Our experiment was performed using a scanning tunnelling microscope (STM) in ultra-high vacuum (UHV) at $T=4.8\,\mathrm{K}$ to probe back-gated devices consisting of chemical vapor deposition (CVD)-grown graphene¹⁶ placed on top of boron nitride (BN) flakes¹⁷ on a SiO₂/Si surface. The use of BN substrates significantly reduces the charge inhomogeneity of graphene^{18,19}, thus allowing us to probe the intrinsic graphene electronic response to individual charged impurities. The charged impurities probed in this work were cobalt trimers constructed on graphene by atomically manipulating cobalt monomers with the tip of an STM (cobalt atoms were deposited via e-beam evaporation onto low-temperature graphene samples). Figure 1a–f shows the process of manipulating three cobalt monomers to create a single Co trimer on graphene (the detailed interior structure of the Co trimer cannot be resolved owing to its instability under high current measurement).

Co trimers were used in this study because they form a robust, reproducible impurity whose charge can be toggled on and off through the use of a back-gate electrode. Co monomers (which can also be charge-toggled) were unsuitable for this study owing

to the fact that their charge state switches in the proximity of an STM tip²⁰ (thus leading to spatially inhomogeneous ionization features that mask the intrinsic graphene response to a Coulomb impurity of fixed charge). Co trimers are ideal because they can be prepared in different charge states (through back-gating) that are charge-stable in the proximity of an STM tip. This is shown in the spectroscopic data of Figs 1g and 2. Figure 1g shows STM spectra acquired with the STM tip held directly over a single Co trimer for two different back-gate voltages (Vg). Following the analysis of ref. 20, the Co trimer impurity state marked R is seen to lie below the Fermi level $(E_{\rm F})$ for $V_{\rm g}=+14\,{\rm V}$, in which case it is filled by an electron, whereas it lies above E_F for $V_g = -2 \text{ V}$, in which case the electron has been removed from the trimer. The R state arises from the local cobalt-graphene hybridization and is undetectable at distances greater than $r_0 = 1.5 \,\mathrm{nm}$ from the trimer centre, demonstrating that short-range cobalt-graphene interactions end at r_0 . The spectroscopic feature marked S arises owing to tip-induced ionization of the trimer and thus confirms the charging nature of the impurity state **R** (refs 20–22).

The gate-dependent charge states of the Co trimer were determined by performing differential conductance (dI/dV) mapping of the surrounding graphene for different trimer charge configurations. Figure 2a shows a map of the trimer in a bistable configuration with $V_g = +13 \,\text{V}$. In this configuration the trimer exhibits a tip-induced ionization ring^{20–22} (that is, the trimer charge state changes by one electron depending on whether the tip is inside or outside the ring feature). In Fig. 2b the impurity state of the trimer (**R** in Fig. 1g) is well below $E_{\rm F}$ ($V_{\rm g} = +45 \, {\rm V}$), and is thus occupied by an electron. In this state the dI/dV map shows no significant structure outside the border of the trimer (that is, for $r > r_0$, where r is distance from the impurity centre), implying that the trimer is in a stable charge-neutral state. In Fig. 2c, however, the impurity state **R** is well above $E_{\rm F}$ ($V_{\rm g} = -20 \, {\rm V}$), and so the trimer is charged here by an amount Q = +1|e| (ref. 20). This charge state is consistent with the long-range radially symmetric contrast in dI/dV signal that is observed in the graphene beyond the border of the trimer. Similar behaviour was reproducibly observed for more than 25 Co trimers (formed both naturally and through atomic manipulation) with ten different tips calibrated against the Au(111) surface state.

Our ability to hold Co trimers in controlled, back-gate determined charge states allows us to measure the energy-dependent electronic local density of states (LDOS) of graphene around well-defined Coulomb impurities. Figure 3a shows the results of such measurements taken at different distances from the

¹Department of Physics, University of California at Berkeley, Berkeley, California 94720, USA, ²Materials Science Division, Lawrence Berkeley National Laboratory, Berkeley, California 94720, USA, ³School of Physics, University of Exeter, Stocker Road, Exeter EX4 4QL, UK, ⁴Department of Physics, Massachusetts Institute of Technology, 77 Massachusetts Ave, Cambridge, Massachusetts 02139, USA. [†]These authors contributed equally to this work. *e-mail: crommie@berkeley.edu.

LETTERS

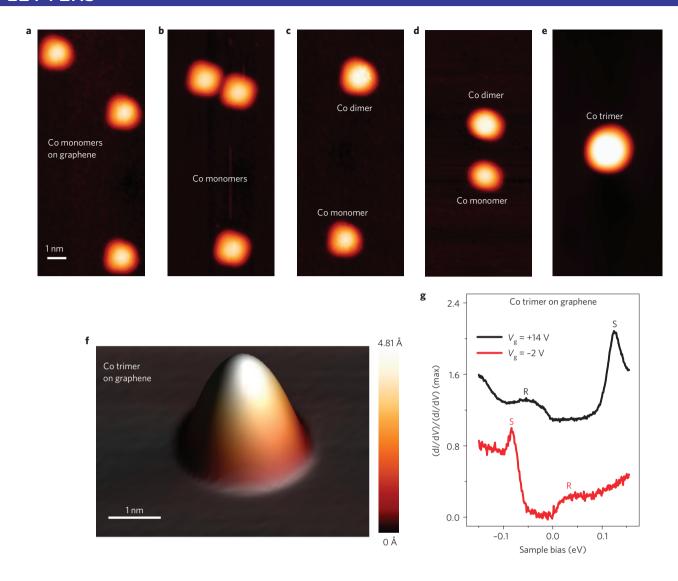


Figure 1 | **Formation, topography and electronic structure of a Co trimer on graphene. a–c,** STM topographs show the process of manipulating two Co monomers to form a Co dimer on a gated graphene device (atomic manipulation parameters: $V_s = +0.48 \text{ V}$, I = 0.050 nA, $V_g = +45 \text{ V}$). **d,e,** STM topographs show the process of manipulating a Co dimer to combine with a monomer for creation of a Co trimer on a gated graphene device (atomic manipulation parameters: $V_s = -0.46 \text{ V}$, I = 0.060 nA, $V_g = -45 \text{ V}$). **f**, Zoom-in STM topograph of a Co trimer on graphene (tunnelling parameters: $V_s = +0.30 \text{ V}$, I = 0.015 nA, $V_g = +30 \text{ V}$). **g**, dI/dV spectra taken with tip directly above the centre of a Co trimer on graphene for different back-gate voltages (initial tunnelling parameters: $V_s = -0.15 \text{ V}$, I = 0.020 nA).

centre of a Co trimer in the charge state Q=+1|e| ($V_{\rm g}=-15\,{\rm V}$). The dI/dV point spectra shown here have each been normalized by a different constant to account for the exponential change in conductivity that occurs at each measurement location as tip height is changed relative to the tip height at a distance far from the impurity^{23,24} (see Supplementary Information for details). All the dI/dV spectra plotted in Fig. 3a show a \sim 130 meV wide gap-like feature at the Fermi level caused by phonon-assisted inelastic tunnelling²⁵, and an additional minimum around $V_{\rm s}=+0.13\,{\rm V}$ which is associated with the Dirac point²⁵. The primary difference between each spectrum is a systematic variation in the filled-state and empty-state intensities as a function of distance from the trimer centre. The empty-state state intensity above the Dirac point increases as the tip nears the trimer, whereas the filled-state intensity below the Dirac point correspondingly decreases.

Experimental dI/dV maps were obtained at different sample biases for the graphene surface surrounding a Co trimer in the Q = +1|e| state. Figure 4a,c plots radial averaged dI/dV linescans

measured as a function of distance from the Co trimer centre. These curves have been normalized to account for the measured change in tip height at different spatial locations (see Supplementary Information). Figure 4a shows that the filled-state LDOS at energies below the Dirac point reduces near the Co trimer, but otherwise has very little spatial structure. The empty-state LDOS at energies above the Dirac point has very different behaviour, as seen in Fig. 4c. Here the LDOS strongly increases as the trimer is neared, and a spatial oscillation that disperses with sample bias can be seen.

These experimental observations can be understood within a theoretical framework that incorporates the response of ultrarelativistic Dirac fermions to a Coulomb potential^{6–9}. In this model the STM measures the LDOS of graphene quasiparticles as they arrange themselves around a charged impurity according to the physics of the massless Dirac equation. We calculated the expected LDOS of graphene at different distances away from a positively charged Coulomb impurity and compared this simulation to our distance-dependent, energy-resolved measurements of graphene

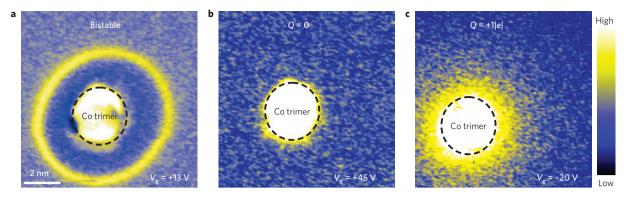


Figure 2 | **Controlling the charge state of a Co trimer on graphene. a**, dI/dV map of graphene near a Co trimer tuned to a bistable charge state using back-gate (tunnelling parameters: $V_s = +0.30 \text{ V}$, I = 0.018 nA, $V_g = +13 \text{ V}$). **b**, dI/dV map of graphene near a Co trimer tuned to a stable Q = 0 charge state using back-gate ($V_s = +0.30 \text{ V}$, I = 0.010 nA, $V_g = +45 \text{ V}$). **c**, dI/dV map of graphene near a Co trimer tuned to a stable Q = +1|e| charge state using back-gate ($V_s = +0.30 \text{ V}$, I = 0.009 nA, $V_g = -20 \text{ V}$).

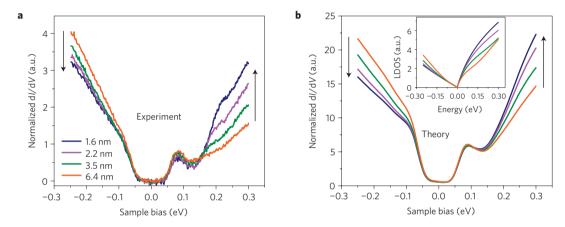


Figure 3 | dI/dV spectra near a charged Co trimer on graphene. **a**, Normalized dI/dV spectra measured on graphene at different distances from the Co trimer centre when the trimer is tuned to charge state Q = +1|e| (initial tunnelling parameters: $V_s = +0.30 \text{ V}$, I = 0.015 nA, $V_g = -15 \text{ V}$, wiggle voltage $V_{rms} = 6 \text{ mV}$). Arrows indicate the direction towards the charged impurity. **b**, Theoretically simulated normalized dI/dV intensity for graphene at the same distances as in **a** for effective impurity charge $Q_{eff} = Q/(\varepsilon_g \varepsilon_s) = (+1|e|)/(3 \times 2.5) = +0.13|e|$. Inset: corresponding simulated bare LDOS of graphene calculated near an impurity having $Q_{eff} = +0.13|e|$.

LDOS around charged Co trimers. Calculations of the LDOS around a Coulomb impurity were carried out using the method of ref. 8. This calculation assumes a two-dimensional continuum Dirac model for undoped graphene in the presence of a Coulomb potential, and the only fitting parameter is the interband dielectric constant, $\varepsilon_{\rm g}$, of undoped graphene. Although the graphene used in our experiment has some finite doping ($\sim 5 \times 10^{11} \, \text{cm}^{-2}$), this model is still valid in proximity to the charged impurity as the effects of free-electron-like screening only become important for distances from the impurity greater than the screening length $\lambda \sim 1/k_{\rm F} = \hbar v_{\rm F}/\varepsilon_{\rm F} \sim 7$ nm (refs 26,27). For $r_0 < r \lesssim \lambda$ screening is dominated by the intrinsic interband contribution to graphene polarization (ε_g), whose main effect is to produce screening charge localized at the impurity centre^{26,27}. The overall charge of the Coulomb potential felt by graphene quasiparticles near the impurity within the screening length is thus reduced to $Q_{\text{eff}} = Q/(\varepsilon_g \varepsilon_s)$, where Q is the bare impurity charge (in this case $Q = +\tilde{1}|e|$) and $\varepsilon_s = (\varepsilon_{BN} + 1)/2 = 2.5$ is the average dielectric constant of the substrates surrounding the graphene (ε_s arises from BN on one side and vacuum on the other).

We find that the data in Fig. 3a (which satisfies $r_0 < r \lesssim \lambda$) is best fit using $\varepsilon_{\rm g} = 3.0 \pm 1.0$. Figure 3b shows the corresponding theoretical ${\rm d}I/{\rm d}V$ spectra calculated for the same distances from the charged impurity centre as measured experimentally. These simulated spectra were obtained from the theoretical Dirac fermion

LDOS (Fig. 3b inset) by rigidly shifting the LDOS in energy to account for finite doping in the experiment, by broadening the LDOS with the finite quasiparticle lifetime, and by including phonon-assisted inelastic tunnelling processes, all according to the method of ref. 28 (the estimated error in our extracted value of $\varepsilon_{\rm g}=3.0\pm1.0$ arises from the standard deviation in $\varepsilon_{\rm g}$ values obtained from different sets of dI/dV spectra, see Supplementary Information). Tip-induced band-bending was not included in our simulations because it is expected to be relatively small for the experimental doping levels used in this study (see Supplementary Informations for details).

As can be seen in Fig. 3b, the experimentally observed spatial dependence of the graphene LDOS around a charged impurity is reproduced well by the simulations. Namely, the LDOS of states above (below) the Dirac point are enhanced (reduced) as one moves closer to the impurity. This electron–hole asymmetry can be qualitatively understood as arising from the positive Coulomb potential of the Co trimer attracting negative charge carriers and repelling positive charge carriers. Our observation that the change in LDOS reduces as the energy nears the Dirac point is qualitatively different from the behaviour expected for a conventional material having parabolic dispersion. This is because the electron–impurity interaction strength (the ratio of electronic potential energy over kinetic energy in the presence of a charged impurity) for graphene is independent of energy, in contrast to the $1/\sqrt{E}$ behaviour expected

LETTERS

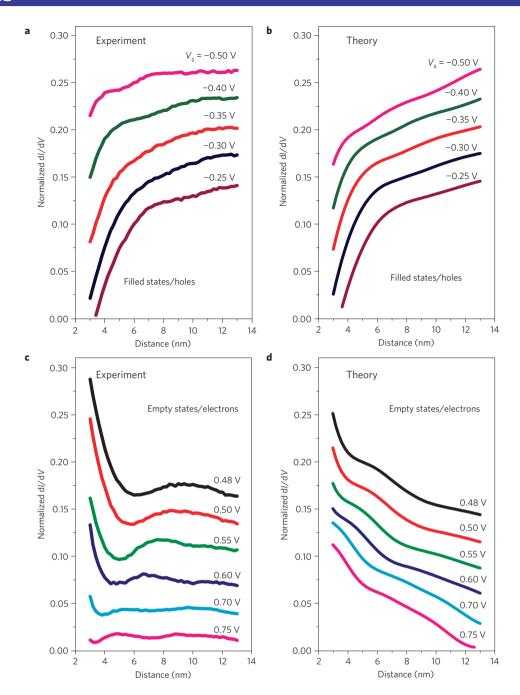


Figure 4 | dI/dV versus distance linescans near a charged Co trimer on graphene. **a**, Experimental distance-dependent radial averaged normalized dI/dV linescans for graphene near a Co trimer with Q = +1|e| charge (filled states, trimer centre at r = 0). All curves are normalized by the value at r = 13 nm and shifted vertically for easier viewing (experimental parameters: $V_g = -15$ V and $(V_s, I) = (-0.50 \text{ V}, 55 \text{ pA}), (-0.40 \text{ V}, 55 \text{ pA}), (-0.35 \text{ V}, 40 \text{ pA}), (-0.30 \text{ V}, 40 \text{ pA}) and (-0.25 \text{ V}, 30 \text{ pA}) from top to bottom under constant current feedback and with wiggle voltage <math>V_{rms} = 8 \text{ mV}$). **b**, Theoretically simulated distance-dependent normalized dI/dV linescans for graphene near a charged impurity having $Q_{eff} = +0.13|e|$ (filled states, impurity centre at r = 0). All theoretical curves are normalized by the value at r = 13 nm. **c**, Experimental dI/dV linescans for graphene near a Co trimer with Q = +1|e| charge (empty states). Curves are plotted as in **a** (experimental parameters: $V_g = -15$ V and $(V_s, I) = (0.48 \text{ V}, 58 \text{ pA}), (0.50 \text{ V}, 58 \text{ pA}), (0.55 \text{ V}, 55 \text{ pA}), (0.60 \text{ V}, 65 \text{ pA}), (0.70 \text{ V}, 90 \text{ pA})$ and (0.75 V, 120 pA) from top to bottom). **d**, Theoretically simulated dI/dV linescans for graphene near a charged impurity having $Q_{eff} = +0.13|e|$ (empty states). Curves are plotted as in **b**.

for this factor in conventional materials²⁷ (see Supplementary Information for a more detailed comparison between graphene and conventional materials). The lack of well-defined resonances in the graphene LDOS off the trimer indicates that no quasibound states are formed around the trimer, consistent with the theory of a subcritical graphene Coulomb impurity^{6–8}. This is qualitatively different from traditional impurity systems involving massive fermions, in which case a Rydberg series of bound states

always form around a Coulomb potential². The value of ε_g , which is measured here by a direct 'test-charge' method, is close to the value calculated using the random phase approximation method^{26,27} ($\varepsilon_{RPA}=2.3$), but is significantly smaller than the value $\varepsilon_g\approx 15$ reported in ref. 29. The small value of ε_g implies that electron–electron interactions should play an important role in graphene¹⁵, consistent with recent experiments reporting Fermi velocity renormalization^{30,31}.

NATURE PHYSICS DOI: 10.1038/NPHYS2379 LETTERS

Further confirmation of this theoretical interpretation of our data is seen in the simulated dI/dV linescan profiles of Fig. 4b,d for graphene surrounding a charged impurity. Here we observe a similar asymmetry in the electron-like and hole-like LDOS of graphene near a charged impurity. The theoretical linescans also reproduce another feature seen in the data, namely the appearance of dispersing spatial oscillations that are stronger in the electron-like LDOS above the Dirac point than in the hole-like LDOS below it. These oscillations arise from the quantum interference of scattered Dirac fermions³². The electron-like interference amplitude is larger because electrons are pulled closer to the positive scattering centre, and so experience a larger effective scattering phase shift than holelike quasiparticles. A difference between experiment and theory is that the theoretical LDOS has a long-range slope that is not seen in the data (that is, for $r \gtrsim 6$ nm). This can be explained by free-electron-like screening for $r > \lambda$ that arises from the finite doping of the experimental graphene. The general asymmetry in electron-hole behaviour observed in this study can potentially explain differences in the mobility seen for electrons versus holes in graphene transport measurements¹⁰.

Methods

The experiments were performed using an Omicron STM under UHV ($P < 10^{-10}$ torr) at 4.8 K. STM tips were calibrated against the Au(111) surface state before all measurements. Differential conductance (dI/dV) was measured by lockin detection of the a.c. tunnel current modulated by a 6–9 mV (root mean squared), 350–500 Hz signal added to the tunnelling bias (V_s). The Co evaporator was first calibrated by evaporating Co atoms onto a Cu(111) surface and then checking the Kondo dip spectroscopic feature to identify individual Co adatoms³³. The graphene sample was grown by the CVD method described in ref. 16. Boron nitride flakes (Momentive Company) were exfoliated onto heavily doped silicon wafers coated in 285 nm thermal oxide. The graphene was placed on top of the BN/SiO₂ (ref. 18) and electrical contact was made by depositing Ti (10-nm thick)/Au (30-nm-thick) electrodes using a stencil mask technique. The graphene sheet is grounded through the electrode. Samples were annealed in UHV at $T \sim 400\,^{\circ}\mathrm{C}$ for several hours to clean them before loading into the STM. Co atoms were then evaporated onto the graphene surface while holding the graphene at low temperature (<10 K).

Received 9 February 2012; accepted 26 June 2012; published online 29 July 2012

References

- Greiner, W., Muller, B. & Rafelski, J. Quantum Electrodynamics of Strong Fields (Springer, 1985).
- Landau, L. D. & Lifshitz, E. M. Quantum Mechanics: Non-relativistic Theory (Pergamon, 1981).
- 3. Zeldovic, Y. B. & Popov, V. S. Electronic structure of superheavy atoms. Sov. Phys. Usp 14, 673–694 (1972).
- Biswas, R. R., Sachdev, S. & Son, D. T. Coulomb impurity in graphene. *Phys. Rev. B* 76, 205122 (2007).
- Novikov, D. S. Elastic scattering theory and transport in graphene. *Phys. Rev. B* 76, 245435 (2007).
- Pereira, V. M., Nilsson, J. & Castro Neto, A. H. Coulomb impurity problem in graphene. *Phys. Rev. Lett.* 99, 166802 (2007).
- Shytov, A. V., Katsnelson, M. I. & Levitov, L. S. Atomic collapse and quasi-Rydberg states in graphene. *Phys. Rev. Lett.* 99, 246802 (2007).
- Shytov, A. V., Katsnelson, M. I. & Levitov, L. S. Vacuum polarization and screening of supercritical impurities in graphene. *Phys. Rev. Lett.* 99, 236801 (2007).
- Terekhov, I. S., Milstein, A. I., Kotov, V. N. & Sushkov, O. P. Screening of Coulomb impurities in graphene. *Phys. Rev. Lett.* 100, 076803 (2008).
- Chen, J. H. et al. Charged-impurity scattering in graphene. Nature Phys. 4, 377–381 (2008).
- 11. McChesney, J. L. et al. Extended van Hove singularity and superconducting instability in doped graphene. *Phys. Rev. Lett.* **104**, 136803 (2010).
- Zhou, S. Y., Siegel, D. A., Fedorov, A. V. & Lanzara, A. Metal to insulator transition in epitaxial graphene induced by molecular doping. *Phys. Rev. Lett.* 101, 086402 (2008).

- 13. Novoselov, K. S. *et al.* Two-dimensional gas of massless Dirac fermions in graphene. *Nature* **438**, 197–200 (2005).
- Zhang, Y., Tan, Y. W., Stormer, H. L. & Kim, P. Experimental observation of the quantum Hall effect and Berry's phase in graphene. *Nature* 438, 201–204 (2005).
- Kotov, V. N., Uchoa, B., Pereira, V. M., Castro Neto, A. H. & Guinea, F. Electron–electron interactions in graphene: Current status and perspectives. *Rev. Mod. Phys.* http://arxiv.org/abs/1012.3484 (2011, in the press).
- Li, X. et al. Large-area synthesis of high-quality and uniform graphene films on copper foils. Science 324, 1312–1314 (2009).
- Dean, C. R. et al. Boron nitride substrates for high-quality graphene electronics. Nature Nanotech. 5, 722–726 (2010).
- Decker, R. et al. Local electronic properties of graphene on a BN substrate via scanning tunneling microscopy. Nano Lett. 11, 2291–2295 (2011).
- 19. Xue, J. et al. Scanning tunnelling microscopy and spectroscopy of ultra-flat graphene on hexagonal boron nitride. *Nature Mater.* **10**, 282–285 (2011).
- Brar, V. W. et al. Gate-controlled ionization and screening of cobalt adatoms on a graphene surface. Nature Phys. 7, 43–47 (2011).
- Marczinowski, F., Wiebe, J., Meier, F., Hashimoto, K. & Wiesendanger, R. Effect of charge manipulation on scanning tunneling spectra of single Mn acceptors in InAs. *Phys. Rev. B* 77, 115318 (2008).
- Pradhan, N. A., Liu, N., Silien, C. & Ho, W. Atomic scale conductance induced by single impurity charging. *Phys. Rev. Lett.* 94, 076801 (2005).
- Li, J., Schneider, W-D. & Berndt, R. Local density of states from spectroscopic scanning-tunneling-microscope images: Ag(111). *Phys. Rev. B* 56, 7656–7659 (1997).
- Wittneven, C., Dombrowski, R., Morgenstern, M. & Wiesendanger, R. Scattering states of ionized dopants probed by low temperature scanning tunneling spectroscopy. *Phys. Rev. Lett.* 81, 5616–5619 (1998).
- Zhang, Y. et al. Giant phonon-induced conductance in scanning tunnelling spectroscopy of gate-tunable graphene. Nature Phys. 4, 627–630 (2008).
- Ando, T. Screening effect and impurity scattering in monolayer graphene. Phys. Soc. Jpn 75, 074716 (2006).
- 27. Hwang, E. H. & Das Sarma, S. Dielectric function, screening, and plasmons in two-dimensional graphene. *Phys. Rev. B* **75**, 205418 (2007).
- Brar, V. W. et al. Observation of carrier-density-dependent many-body effects in graphene via tunneling spectroscopy. Phys. Rev. Lett. 104, 036805 (2010).
- Reed, J. P. et al. The effective fine-structure constant of freestanding graphene measured in graphite. Science 330, 805–808 (2010).
- 30. Elias, D. C. et al. Dirac cones reshaped by interaction effects in suspended graphene. *Nature Phys.* **7**, 701–704 (2011).
- Siegel, D. A. et al. Many-body interactions in quasi-freestanding graphene. Proc. Natl Acad. Sci. USA 108, 11365–11369 (2011).
- 32. Rutter, G. M. *et al.* Scattering and interference in epitaxial graphene. *Science* 317, 219–222 (2007).
- Manoharan, H. C., Lutz, C. P. & Eigler, D. M. Quantum mirages formed by coherent projection of electronic structure. *Nature* 403, 512–515 (2000).

Acknowledgements

Research supported by the Office of Naval Research Multidisciplinary University Research Initiative award no. N00014-09-1-1066 (graphene device preparation and characterization), by the Director, Office of Science, Office of Basic Energy Sciences of the US Department of Energy under contract no. DE-AC02-05CH11231 (STM instrumentation development and measurements), and by the National Science Foundation award no. DMR-0906539 (numerical simulations).

Author contributions

Y.W., V.W.B. and M.F.C. designed the experiment and made the measurements. Q.W., W.R., H-Z.T. and A.Z. facilitated the sample fabrication. A.V.S., L.S.L. and Y.W. carried out the theoretical calculation. Y.W., V.W.B., A.V.S., L.S.L. and M.F.C. carried out the analysis and wrote the paper.

Additional information

Supplementary information is available in the online version of the paper. Reprints and permissions information is available online at www.nature.com/reprints. Correspondence and requests for materials should be addressed to M.F.C.

Competing financial interests

The authors declare no competing financial interests.